RSC Applied Polymers

PAPER

View Article Online
View Journal | View Issue

Cite this: *RSC Appl. Polym.*, 2026, **4**, 736

Development of an adsorption–desorption technique for the recovery of rare-earth metal ions using the phase transition behavior of zwitterionic polymer brushes

Tommy Suhartono Wijaya Tan, Naokazu Idota and Takehiko Tsukahara *

This study synthesized a sulfobetaine-type zwitterionic polymer brush on a porous silica particle (P-SiO_2-poly(DMAPS)) through surface-initiated atom transfer radical polymerization (SI-ATRP) and demonstrated its applicability as an adsorption–desorption material for lanthanide (Ln) ions in aqueous solutions. Appropriate Ln adsorption conditions for P-SiO_2-poly(DMAPS) were established according to the effects of various Ln metal ions on the thermo-responsive behavior of poly(DMAPS) in aqueous solutions. From the adsorption experiments, it was confirmed that P-SiO_2-poly(DMAPS) enabled the complete recovery of all Ln ions from aqueous solutions. The regression analyses of the Langmuir adsorption isotherm curves of Ln ions at 50 °C–70 °C showed that the chemisorption processes of all Ln ions on P-SiO_2-poly (DMAPS) were entropy-driven and occurred spontaneously, while the maximum adsorption capacities of Ln ions decreased as the ionic radii decreased from light to heavy Ln ions. Furthermore, 100% of all Ln ions adsorbed on P-SiO_2-poly(DMAPS) desorbed by simple shaking in a certain concentration of ethylenediaminetetraacetic acid (EDTA) solution. These results prove that this novel Ln adsorption–desorption technique using a zwitterionic polymer brush has great potential in chemical, environmental, and energy fields.

Received 28th July 2025,
Accepted 2nd January 2026

DOI: 10.1039/d5lp00239g

rsc.li/rscapplpolym

1. Introduction

Rare-earth elements (REEs; 15 lanthanides as well as scandium and yttrium) are widely used in various energy, electronics, and metallurgy applications and in the environmental, chemical, and biomedical industries owing to their unique physicochemical properties.[1–3] With the number of applications and the development of green technologies increasing globally, the demand for and production of REEs are also increasing annually. Some researchers have stated that the global demand for REEs will reach over 200 000 tons by 2026, and their demand is increasing at a compound annual growth rate (CAGR) of over 12%.[4] It is assumed that such increases in demand and supply will have adverse effects, including an increase in the end-of-life products, resource depletion, rising prices, and environmental pollution from mining. The recycling of REEs is expected to counter these issues and ensure a sustainable supply.

Much effort has been devoted to separation techniques based on liquid–liquid extraction and solid-phase extraction. The effectiveness of these techniques has been investigated in several areas: REE recovery from mining tails, electronic and electrical wastes (e-wastes), industrial wastewater, and radioactive wastes produced from nuclear fuel reprocessing processes, including through the decommissioning of the Fukushima Daiichi nuclear power station.[5–9] Liquid–liquid extraction using specific extractants containing organophosphorus and diglycolamide derivative ligands has demonstrated the efficient and selective recovery of trivalent lanthanide (Ln) ions from aqueous and acidic media.[9–11] However, this method has environmental and safety disadvantages such as time-consuming chemical operations, production of hazardous secondary wastes, and fire and explosion risks. Solid-phase extraction, which involves the adsorption of target metal ions onto solid adsorbents, has been widely recognized as a superior method to liquid–liquid extraction because of its higher separation efficiency and lower solvent volume requirements. Various adsorbents have been developed, such as extractant-impregnated porous silica and surface-functionalized materials, and their abilities to adsorb Ln ions from solutions have been explored.[8,12–16] Some of these adsorbents have accurately separated Ln ions from trivalent minor actinides (MAs) in solutions as well as enabled the mutual separation of Ln ions.[17–21] Porous materials, such as metal–organic frame-

Laboratory for Zero-Carbon Energy, Institute of Integrated Research, Institute of Science Tokyo, 2-12-1-N1-6, Ookayama, Meguro, Tokyo 152-8550, Japan.
E-mail: ptsuka@zc.iir.isct.ac.jp; Tel: +81-3-5734-3067

works (MOFs), covalent organic frameworks (COFs), and porous organic polymers (POPs), are also gaining growing interest as advanced adsorbents for facilitating the efficient separation of radionuclides because of their large specific surface areas, high porosities, controllable pore structures and sizes, and tunable surface functionalities, and their separation abilities for various radionuclides are being investigated.[22] However, existing solid extraction methods have certain drawbacks. For example, they require the introduction of coordination sites that are dedicated to the targeting of Ln ions onto the adsorbents and prolonged stepwise operations, including pretreatment, using different eluents. Accordingly, to solve the problems associated with traditional separation methods, it is essential to develop new separation methodologies for REEs.

In recent years, zwitterionic polymers, bearing positive and negative charges simultaneously on their backbone chain units, have attracted much attention as promising alternatives to existing adsorptive materials because both cations and anions in solutions can be chemically adsorbed onto these polymers. The removal of heavy metal ions from contaminated water has been demonstrated using various zwitterionic polymer derivatives, indicating that their unique properties, such as strong dipole moments and electrostatic interactions, enable them with improved adsorption capacity and selectivity for metal ions.[23–26] Since zwitterionic polymers exhibit a strong salt-responsive anti-polyelectrolyte effect, their structure and conformation are strongly affected by the type and concentration of metal salts. Zwitterionic polymers collapse in water due to the electrostatic inter-/intra-chain bridging of strong dipole–dipole interactions. The introduction of counterions in solutions induces the breaking of the chain bridges, generating more hydrated and stretched polymer chains. Several studies have found that the degree of polymer conformational changes by anions follows the classic Hofmeister series effect, while the ion-screening effect, where cations shield the negative charges within the zwitterionic fragments, is the dominant factor rather than the Hofmeister series effect in the case of cations.[27–32] In particular, the anti-polyelectrolyte effects of monovalent and multivalent metal ions (Na^+, Mg^{2+}, Ca^{2+}, and Y^{3+}) on zwitterionic polymer brushes, where the organic polymer is grafted densely onto the inorganic substrate, have been investigated. The stronger ion-screening effect of polymer brushes has been shown to increase with increasing valence numbers of metal ions.[27] The strong interactions of trivalent Y^{3+} with polymer units can act beyond the anti-polyelectrolyte effect depending on the concentration, causing polymer brush shrinkage. Zwitterionic polymer hydrogels have also been studied. It was found that the adsorption capacity of trivalent Al^{3+} is greater than that of mono- and di-valent metal ions.

The strong effect of multivalent ion addition on polymers has been observed even for polyelectrolyte brushes. In salt environments, polyelectrolyte brushes show the opposite behavior to that of zwitterionic polymers. This is called the polyelectrolyte effect. The brushes collapse due to the adhesion of the counterions to the charged chain units. Because of the high charge density of trivalent La^{3+}, attributed to its small ionic radius, the adhesion strength of La^{3+} on polyelectrolyte brushes is considerably higher.[33–35]

These facts let us hypothesize that the selective adsorption of Ln ions could be feasible owing to slight variations in the interaction between the zwitterionic polymer brushes and each lanthanide with differing ionic radii; moreover, the adsorbed Ln ions could be desorbed by controlling the external solution environments. However, little research has been conducted on the mutual separation of Ln ions using the unique properties of zwitterionic polymer brushes. Their potential for Ln recovery from aqueous solutions should be explored for establishing new approaches for the recycling of REEs and MAs, wastewater treatment, and nuclear waste management. In this study, we aim to demonstrate the recovery of Ln ions from aqueous and acidic solutions using zwitterionic polymer brushes and evaluate their adsorption thermodynamics for Ln ions. We also intend to elucidate the optimal desorption conditions for the recovery of Ln ions adsorbed on zwitterionic polymer brushes. A sulfobetaine-type zwitterionic polymer was grafted onto a porous silica particle because of its superior coordination ability with trivalent metal ions.[27,28] This approach, enabling the capture and recovery of target Ln ions driven by the anti-polyelectrolyte effect, is a facile, safe, and green separation method.

2. Experimental

2.1. Materials

Porous silica (P-SiO_2; CARiACT Q-10, pore size = 10 nm, surface area = 200 m^2 g^{-1}; Fuji Silysia Chemical Ltd) prepared by the sol–gel method was used as a backbone material for the immobilization of polymer brushes. Its surface was activated with a 1 mol% aqueous solution of sodium hydroxide at 60 °C for 24 h. [2-(Methacryloyloxy)ethyl]dimethyl-(3-sulfopropyl) ammonium hydroxide [DMAPS; purity ≥ 95.0%, Sigma-Aldrich] was used as a sulfobetaine-type zwitterionic monomer without purification. 3-(Trichlorosilyl) propyl-2-bromo-2-methylpropanoate ($SiCl_3$-PrBrMePA) and ethyl 2-bromoisobutyrate (EBiB) (purity ≥ 95.0%, Tokyo Chemical Industry Co., Ltd) were directly used as initiators for fabricating the polymer brush and linear polymer, respectively. 2,2′-Bipirydil (purity ≥ 99%, Sigma-Aldrich) was used as a ligand for polymerization. Copper(I) bromide (purity ≥ 99%, Sigma-Aldrich), purified by reacting with acetic acid, and copper(II) bromide (purity ≥ 99%, Sigma-Aldrich), without further purification, were used as catalysts. All Ln nitrate hydrates ($Ln(NO_3)_3{\cdot}nH_2O$; Ln = La, Ce, Pr, Nd, Sm, Eu, Gd, Tb, Dy, Ho, Er, Tm, Yb, and Lu; n = 4–6) were used as received (Wako Pure Chemical Industries, Ltd, Sigma-Aldrich, and Kanto Chemical Co., Inc.).

2.2. Syntheses of linear poly(DMAPS) and the poly(DMAPS) brush

Synthesis of linear polymer [poly(DMAPS)]. The procedure is illustrated in Scheme S1. Atom-transfer radical polymerization (ATRP) was performed in an argon (Ar)-filled glove box.

13.2 mg of copper(I) bromide, 2.3 mg of copper(II) bromide, and 32.0 mg of 2,2′-bipyridyl were introduced into a 50 mL polypropylene (PP) tube with a 12 mL water/methanol mixture (3 : 1 volume ratio) degassed by Ar bubbling. The sample solution was heated to 60 °C, and then, 5.7 g of DMAPS, as the monomer, and 15.0 μL of EBiB, as the ATRP initiator, were added. After heating and stirring for 15 h, the reacted sample solution was diluted with hot water and passed through an alumina column to remove the catalyst. The obtained solution was then evaporated and concentrated under reduced pressure and mixed with a small amount of acetone. By introducing the solution dropwise to diethyl ether, linear poly(DMAPS) could be recovered as a white-colored solid precipitate. It was then dried under vacuum and stored in a refrigerator.

Synthesis of the poly(DMAPS) brush grafted on P-SiO_2 [P-SiO_2-poly(DMAPS)]. Surface-initiated atom-transfer radical polymerization (SI-ATRP) was performed in an argon (Ar)-filled glove box. The fabrication procedures are illustrated in Scheme 1. The surface-activated P-SiO_2 was mixed with anhydrous toluene containing $SiCl_3$-PrBrMePA at 60 °C and stirred for 2 h. After the mixture was suction-filtered and washed repeatedly with anhydrous toluene and anhydrous methanol, the SI-ATRP initiator, PrBrMePA-immobilized P-SiO_2, called the P-SiO_2-initiator, was obtained and dried at 70 °C for 2 h under vacuum. The reaction solution for SI-ATRP was prepared following the same procedures as for ATRP, and the P-SiO_2-initiator (1.0 g) was added to the solution. After heating and stirring at 60 °C for 15 h, the reaction was stopped by exposure to air. The solid matrix was recovered by suction filtration, washed with hot water, added to 0.1 M hydrochloric acid and stirred without heating for 1 h to remove the residual catalyst, resulting in a white powder of P-SiO_2-poly(DMAPS).

2.3. Characterization of linear poly(DMAPS) and the poly (DMAPS) brush

The chemical structures and molecular weight distributions of the synthesized linear poly(DMAPS) were determined using a ^{1}H-NMR spectrometer (JNM-ECX400P, JEOL Ltd) and a gel permeation chromatography (GPC) system equipped with a refractive index detector (RI-2031, JASCO Corp.), respectively. In the GPC system, a mixture of NaH_2PO_4 (0.2 mol L^{-1}) and $NaNO_3$ (0.01 mol L^{-1}) at pH 7 was used as the mobile phase solvent for determining the molecular weight of the linear poly (DMAPS) sample. Meanwhile, in order to determine the molecular weight of the poly(DMAPS) brush, the P-SiO_2-poly (DMAPS) solid matrix was dissolved in a hydrofluoric acid (HF) solution for 3 h under continuous stirring, followed by neutralization of the resulting solution by adding excess sodium carbonate (Na_2CO_3). The neutralized solution was filtered and dialyzed through a dialysis membrane for 3 days, followed by freeze-drying. The recovered sample was dissolved in $NaNO_3$ (0.2 mol L^{-1}), which was used as the mobile phase solvent, and GPC measurements were performed. The flow rate and the column temperature were set at 0.5 mL min^{-1} and 40 °C for both the linear poly(DMAPS) and poly(DMAPS) brush samples. Polyethylene glycol (Sigma-Aldrich) with molecular weights (M_ws) of 1500, 3000, 6000, 12 000, 40 000, and 107 000 Da were used as standard samples for making calibration curves.

The solid matrixes, such as the P-SiO_2-poly(DMAPS), were characterized by Fourier-transform infrared spectroscopy (FT-IR-4100, JASCO Corp.). Thermogravimetric differential thermal analysis (TG-DTA; DTG-60H, Shimadzu Co., Japan.) was also carried out on the P-SiO_2-poly(DMAPS) and P-SiO_2-initiator from ambient temperature to 800 °C at a heating rate

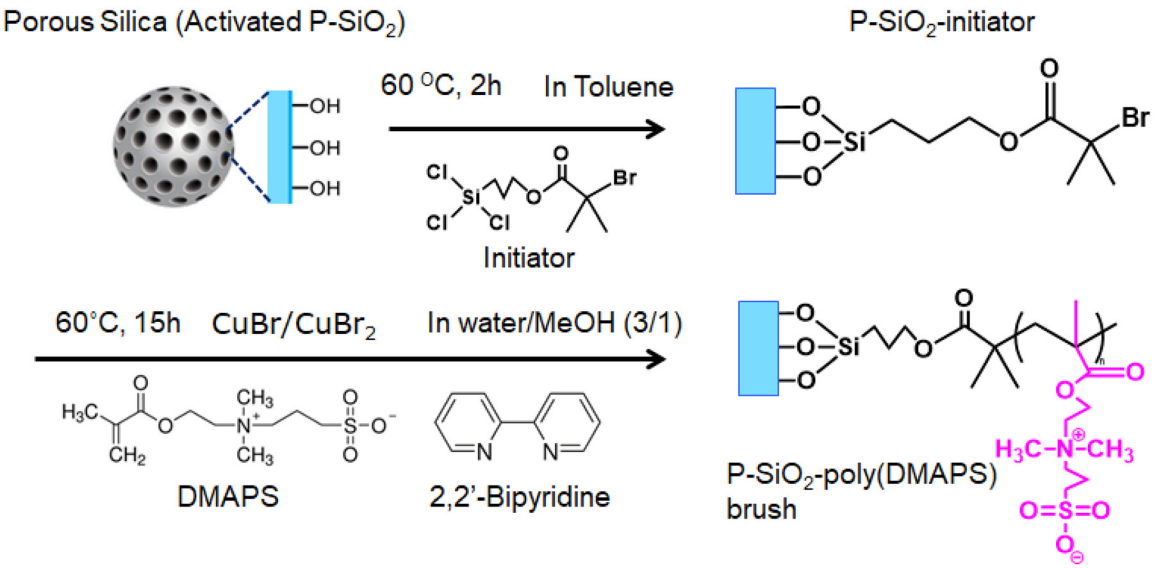

Scheme 1 Schematic of the synthesis procedures for P-SiO_2-poly(DMAPS).

of 5 °C min^{-1} under air flow to determine the weight losses of substances immobilized on the surfaces. The morphologies of the P-SiO_2-poly(DMAPS) before and after the adsorption experiments were observed by scanning electron microscopy (SEM; TM3000, Hitachi Ltd, Japan).

2.4. Determination of the UCST of linear poly(DMAPS) and the poly(DMAPS) brush

Zwitterionic polymers exhibit a thermo-responsive feature of hydrophobic-hydrophilic switching by phase transition across the upper critical solution temperature (UCST). It has been shown that UCST varies depending on the concentration of monovalent salts such as NaCl.[36–39] Although little information is available on the effects of multivalent ions, they may induce greater effects than monovalent ions on UCST. Accordingly, to facilitate Ln adsorption tests, it is necessary to examine the UCST of aqueous polymer solutions containing Ln ions and identify the appropriate temperature conditions. The accurate determination of the effects of metal ions on the UCST of poly(DMAPS) can be achieved by examining the changes in the optical transmittances of aqueous solutions containing linear poly(DMAPS) at an optimal concentration. The optical transmittances of aqueous polymer solutions at 500 nm were measured by means of a UV-Vis spectrophotometer (V-630, JASCO Co.) equipped with a Peltier thermostatted cell holder (control accuracy: ±0.1 °C, speed: 1 °C min^{-1}) at temperatures ranging from 0 °C to 60 °C. All temperature-dependent transmittances were examined under the cooling process because of the presence of hysteresis, as shown in Fig. S1.

In order to identify the optimal polymer concentration, temperature-dependent transmittance measurements were performed for linear poly(DMAPS) solutions dissolved in ultrapure water (Direct-Q3 system, Millipore Co.) at concentrations ranging from 1 mg mL^{-1} to 50 mg mL^{-1}. Further, the temperature at which the optical transmittance began to decrease from nearly 100% during the cooling process was identified as the clearing-point temperature (T_c). T_c was measured because UCST often corresponds to the maximum T_c obtained upon varying the polymer concentrations. Results are shown in Fig. 1(a). At poly(DMAPS) concentrations ranging from 1 to 5 mg mL^{-1}, the solutions transitioned from transparent to opaque, suggesting a reduction in transmittance from 100% with decreasing temperature. On the other hand, when poly(DMAPS) concentrations exceeded 10 mg mL^{-1}, the turbidities of the aqueous polymer solutions became too high, resulting in the transmittances failing to reach 100% even under high temperatures. From the plots of the obtained T_c values against poly(DMAPS) concentrations (Fig. 1(b)), it seems that the maximum T_c appears to be at 22 °C for the poly(DMAPS) concentrations of 10 mg mL^{-1} or more. However, such high-concentrated polymer solutions, in which the transmittances cannot reach 100%, are completely unsuitable for UCST determination. Therefore, 5 mg mL^{-1}, which enables the transmittance change from 100% to 0%, was selected as the optimal poly(DMAPS) concentration in this study.

The sample solutions were prepared by dissolving linear poly(DMAPS) (5 mg mL^{-1}) and each of the metal salts, such as KNO_3, $CsNO_3$, $Mg(NO_3)_2$, $Sr(NO_3)_2$, and $La(NO_3)_3$, into ultrapure water. Moreover, the effects of La^{3+} concentration (3.1×10^{-9} to 1×10^{-1} M) and Ln ionic radii ($Ln^{3+} = La^{3+} \sim Lu^{3+}$, 1×10^{-4} M) on poly(DMAPS)'s UCST were investigated using poly(DMAPS)'s concentration at 5 mg mL^{-1}.

Moreover, UCST determination for the poly(DMAPS) brush was conducted by differential scanning calorimetry (DSC: DSC-60 Plus, Shimadzu). After the synthesized P-SiO_2-poly(DMAPS) was dispersed in ultrapure water solution (±5–10 mg in 50 μL water), the prepared sample was added to an aluminum pan and sealed with an aluminum cover. The temperatures were varied from 0 °C to 60 °C, and the DSC curves were measured under heating and cooling processes at a rate of 2 °C min^{-1}.

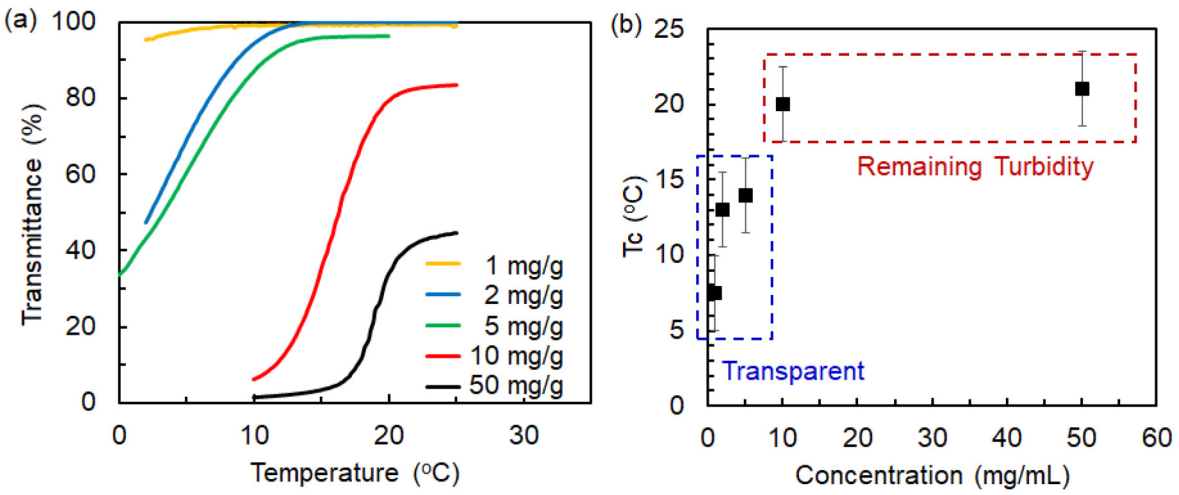

Fig. 1 (a) Plots of temperature dependence of optical transmittance for linear poly(DMAPS) at concentrations from 1 to 50 mg mL^{-1} and (b) plots of the obtained clearing-point temperature (T_c) values against the concentrations of linear poly(DMAPS).

2.5. Adsorption/desorption experiments

Adsorption/desorption experiments of Ln ions by P-SiO_2-poly (DMAPS) were carried out as follows. As the sample solutions for Ln adsorption, $Ln(NO_3)_3$ solutions (Ln = La to Lu) were prepared at various concentrations. The sample solutions (of 10 mL each) were individually poured into PP tubes at temperatures above UCST (50 °C–70 °C), at which poly(DMAPS) was able to show hydrophilicity even in Ln ion-containing solutions, and 100 mg of P-SiO_2-poly(DMAPS) was added to each tube. After the mixed solution was shaken for 60 min to reach the adsorption equilibrium state, 1 mL of supernatant was passed through a syringe with a filter and diluted with 2% HNO_3. The Ln concentrations in the diluted solutions were measured by inductively coupled plasma mass spectrometry (ICP-MS; NexION 300X, PerkinElmer, Inc.). The Ln adsorption ratios were determined by calculating the ratio of the initial Ln ion concentration ($[Ln]_0$) and the Ln concentration adsorbed on the polymer brush ($[Ln]_{ads}$), as shown in eqn (1):

$$\text{Adsorption ratio}(\%) = \frac{[Ln]_{ads}}{[Ln]_0} \times 100\% = \frac{[Ln]_0 - [Ln]_{remain}}{[Ln]_0} \times 100\%, \quad (1)$$

where $[Ln]_{remain}$ corresponds to the Ln ion concentration remaining in the solution after adsorption.

All the remaining solutions after the adsorption experiments were removed from the tubes using syringe filters, leaving only the Ln ion-adsorbed P-SiO_2-poly(DMAPS) solid matrixes in the tubes. In order to desorb Ln ions from the solid matrixes, the desorption reagents (10 mL in quantity) were added into the tubes and shaken for 60 min at temperatures below the UCST (5 °C–10 °C) of the poly(DMAPS). Since poly(DMAPS) exhibits hydrophobic properties at these temperatures, the re-adsorption of Ln ions onto the polymer brush can be prevented. Aqueous solutions containing various concentrations of HNO_3, HCl, diethylenetriamine (Dien), and ethylenediaminetetraacetic acid (EDTA) were used as desorption reagents because acidic solutions such as HNO_3 and HCl are typical eluents and Dien and EDTA are expected to form low-toxicity water-soluble chelate complexes with Ln ions.[40,41] 1 mL of supernatant obtained from each desorption operation was passed through a syringe filter and diluted with 2% HNO_3. ICP-MS measurements were then performed. The desorption ratios were determined according to eqn (2):

$$\text{Desorption ratio}\,(\%) = \frac{[Ln]_{release}}{[Ln]_{ads}} \times 100\%, \quad (2)$$

where $[Ln]_{ads}$ and $[Ln]_{release}$ represent the Ln ion concentration adsorbed on the polymer brush and the Ln ion concentration in solution released from the polymer brush after desorption treatment, respectively.

3. Results and discussion

3.1. Characterization of the synthesized linear poly(DMAPS) and the poly(DMAPS) brush

The ^{1}H-NMR spectra of the DMAPS monomer and the synthesized linear poly(DMAPS) are shown in Fig. S2. Two characteristic peaks were observed at around 5.7 and 6.1 ppm, assigned to the vinyl group of the DMAPS monomer, which disappeared after the polymerization reaction. Meanwhile, the peaks originating from the main chains of poly(DMAPS) appeared at around 1.0 ppm. The peaks assigned to the functional groups other than the vinyl group in DMAPS became broader overall after polymerization. The ^{1}H-NMR spectral changes indicate that poly(DMAPS) was synthesized. The GPC measurement of the synthesized linear poly(DMAPS) showed weight-average (M_w) and number-average (M_n) molecular weights of 77 900 and 38 900, respectively. The polydispersity index (PDI) and the degree of polymerization (DP) of linear poly(DMAPS) became 2.0 and 278, respectively. It was found that the uniformity of linear poly(DMAPS) was not very high, but it had a sufficient molecular weight for the determination of UCST. These ATRP results implied that poly(DMAPS) can be grafted similarly onto P-SiO_2 by means of SI-ATRP using a structurally analogous initiator. On the other hand, the GPC measurement of the poly(DMAPS) brush stripped from the P-SiO_2 surface by HF treatment showed an M_w of 13 160 and M_n of 9 734. The PDI and DP values were determined to be 1.352 and 47, respectively. The smaller PDI and DP values of the poly(DMAPS) brush obtained *via* SI-ATRP than that of the linear poly(DMAPS) could be attributed to the limitations on polymer chain mobility and monomer diffusion onto the grafted polymer layers. These limitations cause both the inhibition of the propagation reaction and an increase in the termination probability, resulting in the formation of shorter polymer chains than linear poly(DMAPS) grafted on the P-SiO_2 surfaces. In addition, the grafting density of the poly(DMAPS) brush could be calculated using the relationship between the M_n value and the number of chains per gram of P-SiO_2 and area of P-SiO_2 according to eqn (S1)–(S3) in the SI, yielding a value of 0.1533 chains per nm^2. These results indicate that the poly(DMAPS) brush synthesized *via* SI-ATRP is suitable for Ln adsorption experiments.

Characterization of the P-SiO_2-poly(DMAPS) was performed using SEM, FT-IR spectroscopy, and TG-DTA technique. The SEM images of bare P-SiO_2 and P-SiO_2-poly(DMAPS) are shown in Fig. 2(a). Although bare P-SiO_2 comprised aggregates of small primary particles of 1–10 nm scale, P-SiO_2-poly(DMAPS) was covered with the polymer grafted on P-SiO_2 surfaces. Fig. 2(b) shows the FT-IR spectra of bare P-SiO_2 and the P-SiO_2-poly(DMAPS). Typical peaks attributed to the Si-CH_3 rocking mode and Si–O–Si stretching mode of the P-SiO_2 backbone were observed at around 790 cm^{-1} and 1050–1250 cm^{-1}, respectively, for the bare P-SiO_2 and P-SiO_2-poly(DMAPS) samples. The P-SiO_2-poly(DMAPS) sample showed characteristic peaks corresponding to the S═O stretching and C═O stretching of poly(DMAPS) at 1035 cm^{-1} and 1716 cm^{-1},

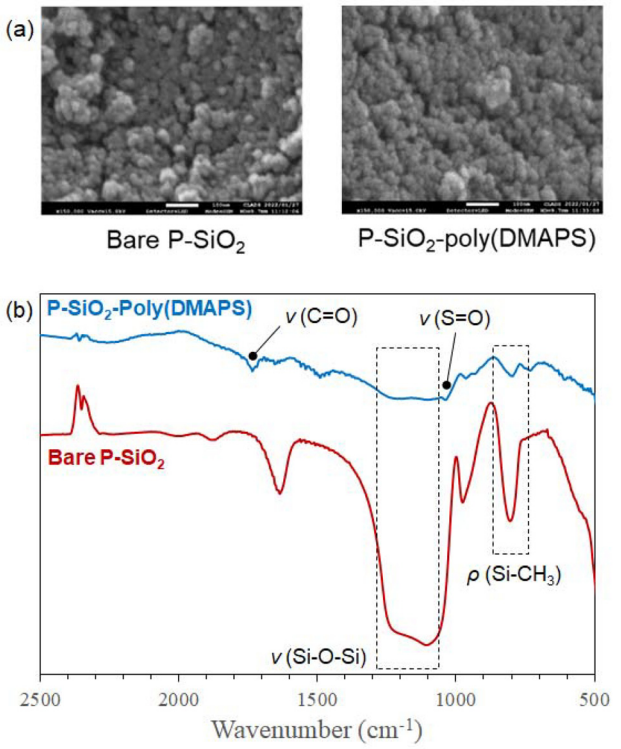

Fig. 2 (a) SEM images of bare P-SiO_2 and P-SiO_2-poly(DMAPS) and (b) FT-IR spectra of bare P-SiO_2 and P-SiO_2-poly(DMAPS).

respectively, indicating the immobilization of poly(DMAPS) on the P-SiO_2 surface.

TG-DTA analysis provided a qualitative determination of the amount of organic materials immobilized on the P-SiO_2 surface. The TG-DTA curves of the P-SiO_2-initiator and P-SiO_2-poly(DMAPS) samples are presented in Fig. 3. Gradual and drastic weight losses were observed in the TG curves of both samples in the ranges of 20–100 °C and 250–400 °C, respectively. At similar temperature ranges, there were endothermic and exothermic peaks in the DTA curves. The endothermic peaks that appeared at about 80 °C for both samples are attributed to the loss of water adsorbed on the surfaces. Meanwhile, the exothermic peaks at 280 °C for the P-SiO_2-initiator and at 360 °C for P-SiO_2-poly(DMAPS) can be ascribed to the decomposition of the initiator and poly(DMAPS), respectively. Therefore, the amounts of the initiator and poly(DMAPS) immobilized on P-SiO_2 were determined from the weight losses in the TG curves between 250 °C and 800 °C. It was observed that the weights of the P-SiO_2-initiator (15.59 mg) and P-SiO_2-poly(DMAPS) (13.29 mg) at 250 °C decreased to 13.82 mg and 7.055 mg, respectively, at 800 °C. The weight loss of 1.77 mg for the P-SiO_2-initiator meant that 0.128 mg of the initiator immobilized per mg of the P-SiO_2 particle was decomposed. In addition, since 6.235 mg of the initiator bearing poly(DMAPS) on P-SiO_2-poly(DMAPS) was burnt, leaving 7.055 mg of P-SiO_2, the initiator that can be immobilized on 7.055 mg of P-SiO_2 was estimated to be 0.903 mg, in accordance with 0.128 mg per mg-P-SiO_2. The weight difference between the initiator and initiator-bearing poly(DMAPS) was found to be 5.332 mg of poly(DMAPS) per P-SiO_2-poly(DMAPS) (13.29 mg). Considering the molecular weight of the DMAPS monomer (279.35 g mol^{-1}), the amount of the DMAPS monomer on P-SiO_2-poly(DMAPS) was determined as 1.27 mmol g^{-1}. These P-SiO_2-poly(DMAPS) matrixes were used for the adsorption/desorption experiments on Ln ions.

3.2. Evaluation of the UCST changes in linear poly(DMAPS) and the poly(DMAPS) brush

The effects of metal ions on the UCST of poly(DMAPS) were investigated by optical transmittance measurements. Fig. 4(a) shows the temperature-dependent optical transmittance plots for poly(DMAPS) (5 mg mL^{-1}) in ultrapure water and in aqueous solutions containing various metal ions (1×10^{-4} M). The T_c of poly(DMAPS) in pure water was about 14 °C, which was almost consistent with those in aqueous solutions containing monovalent cations (K and Cs; 1×10^{-4} M). These transmittance changes occurred gradually, and negative temperatures were needed to achieve 0% transmittance. When multivalent cations were added to the water containing polymer, the T_c value of the polymer was shifted to higher temperatures. The T_c values were determined to be 16 °C–

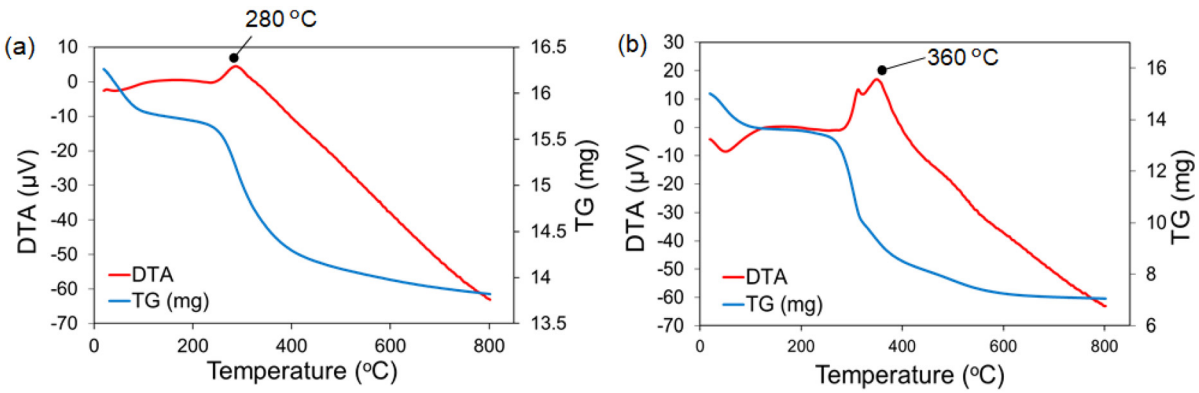

Fig. 3 TG-DTA curves of (a) P-SiO_2-initiator and (b) P-SiO_2-poly(DMAPS).

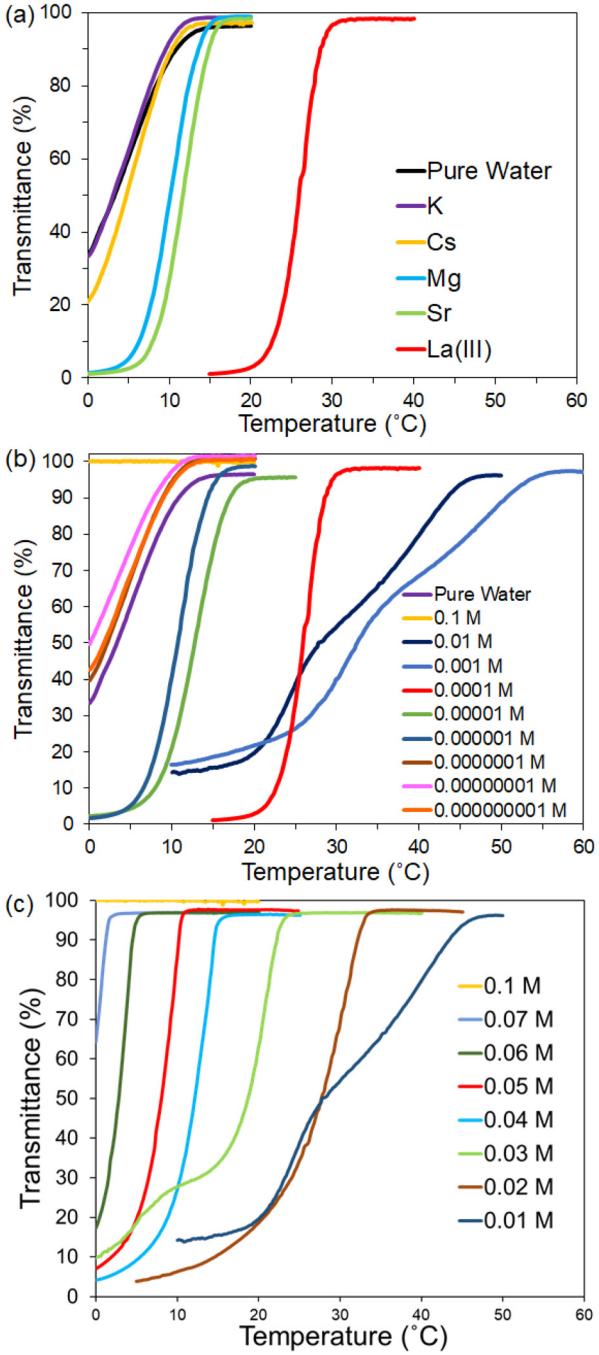

Fig. 4 Plots showing the temperature dependence of optical transmittance for poly(DMAPS) in (a) ultrapure water and aqueous solutions containing various metal ions and aqueous solutions containing La ions at concentrations of (b) 1×10^{-9} M–0.1 M and (c) 0.01–0.1 M.

17 °C and about 31 °C for divalent ions (Mg and Sr; 1×10^{-4} M) and trivalent ions (La; 1×10^{-4} M), respectively. In addition, the phase transition occurred sharply due to the rapid response of the polymer to temperature changes. These results indicated that the addition of multivalent cations induced stronger anti-polyelectrolyte effects, improving the wettability of poly(DMAPS).

The dependence of the poly(DMAPS)'s UCST on La(III) concentration was examined in the concentration range from 1×10^{-9} M to 0.1 M. Plots of transmittance against temperature for each polymer solution are shown in Fig. 4(b) and (c). Each figure corresponds to the plots for a wide La concentration range and for the high La(III) concentration range focusing within 0.01–0.1 M, respectively. As shown in Fig. 4(b), the polymer solutions containing La concentrations from 1×10^{-9} M to 1×10^{-7} M exhibited a similar UCST curve to that of ultrapure water and shifted to higher temperatures with increasing La(III) concentrations. At 1×10^{-4} M, the phase transition behavior was quite sharp, and the T_c value reached about 33 °C. The increase in La(III) concentration from 1×10^{-4} M to 1×10^{-3} M caused a drastic increase in the T_c value to 57 °C, accompanied by a broad phase transition. On the other hand, with further increase in La concentrations, the T_c values shifted inversely to lower temperatures and sharp phase transition states were observed (Fig. 4(c)). The dependence of T_c on La(III) concentration is shown in Fig. S3. It was found that the T_c values moved to lower temperatures than that of ultrapure water, reaching 2 °C at 0.07 M and then at 0.1 M, the T_c could no longer be observed as it constantly provides 100% transmittance across all temperature. The T_c value of poly(DMAPS) in all other Ln ions (Ce to Lu) was further examined, and there were no clear differences in the T_c values with respect to the Ln ionic radii (see Fig. S4), and the T_c value of each Ln-containing poly(DMAPS) was about 30 °C–35 °C. These results imply that poly(DMAPS) is fully capable of adsorbing Ln ions (at concentration in the vicinity of 1×10^{-4} M) under a superior anti-polyelectrolyte effect.

The phase transition temperature of the poly(DMAPS) brush grafted on P-SiO_2 was directly measured by DSC. As shown in Fig. 5, characteristic endothermic and exothermic peaks were observed during the cooling and heating processes, respectively. The temperatures corresponding to the peaks were determined as the phase transition temperatures of the poly(DMAPS) brush, which were 17.78 °C and 41.09 °C for cooling and heating processes, respectively. The hysteresis in the thermally induced phase transition could be attributed to the differences in the conformational transitions in the poly(DMAPS) brush. During the cooling process, the hydrophilic poly(DMAPS) brush in an expanded state could rapidly undergo a phase transition and form aggregates. On the other hand, a significant change from the collapsed state to the expanded state of the poly(DMAPS) brush was required during the heating process. The conformational change of the polymer was invoked by the cleavage of intra-/inter-polymer-chain interactions, resulting in an increase in the transition temperature and release of heat. The transition temperature of 17.78 °C obtained in the cooling process for the poly(DMAPS) brush was similar to the T_c value of about 14 °C for linear poly(DMAPS) (see Fig. S1), but the transition temperatures for the poly(DMAPS) brush (41.09 °C) and linear poly(DMAPS) (T_c = 20 °C) were entirely different from each other. The high polymer density in the poly(DMAPS) brush would be a factor responsible for its higher transition temperature than that of

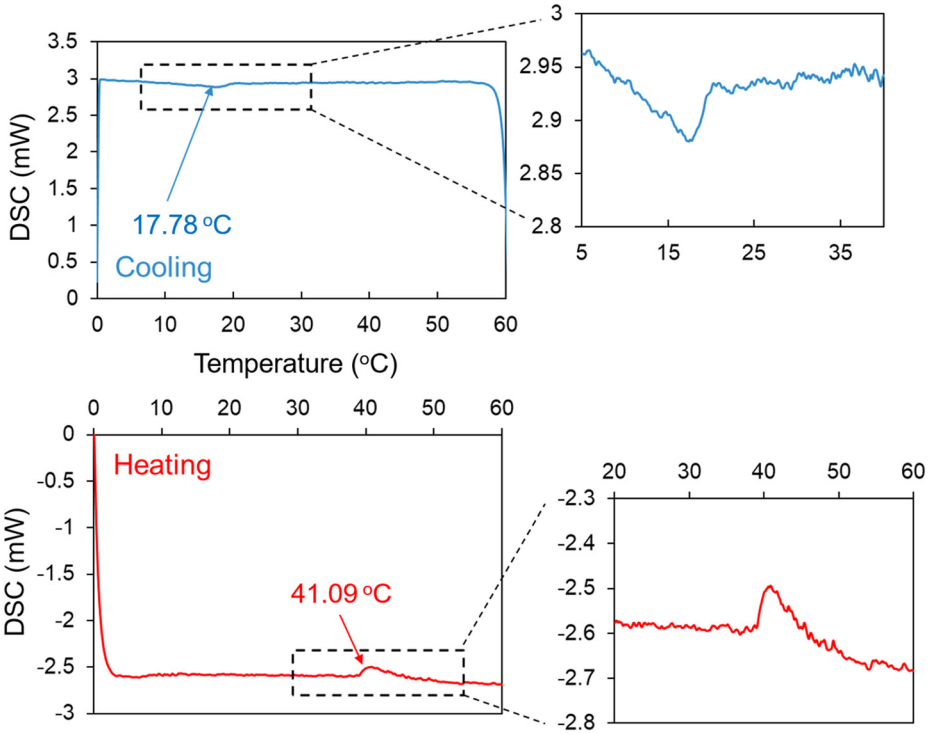

Fig. 5 DSC curves of the P-SiO_2-poly(DMAPS) measured by cooling and heating processes.

linear poly(DMAPS). In this study, UCST and Ln adsorption tests were conducted under the cooling process, in which the poly(DMAPS) brush and linear poly(DMAPS) exhibited similar characteristics.

3.3. Adsorption of lanthanide ions by the poly(DMAPS) brush

Adsorption experiments were conducted at temperatures of 50 °C–70 °C and at various Ln concentrations. As shown in Fig. 6(a)–(c), P-SiO_2-poly(DMAPS) exhibited 100% adsorption ratios at all temperatures at an Ln concentration of 0.1 ppm. For all other Ln concentrations, the adsorption ratios decreased gradually with increasing atomic numbers; at a Lu concentration of 0.3 ppm and 50 °C, the adsorption ratio for Lu was 54.8%, which was almost ten percentage lower than that of La (65.1%) under same conditions. This observation clearly indicated that the adsorption properties of Ln ions on P-SiO_2-poly(DMAPS) differ depending on the Ln species.

Therefore, the adsorption capacities of Ln ions were determined at each temperature using initial Ln(III) concentrations from 0.1 ppm to 1 ppm, and an adsorption isotherm study was performed. The Langmuir and Freundlich adsorption isotherm model fittings are effective means for evaluating adsorption properties at equilibrium conditions and the corresponding adsorption mechanisms.[42,43]The Langmuir isotherm model is applicable to adsorption equilibrium systems satisfying the following assumptions: (1) a finite number of structurally homogeneous and energetically equivalent adsorption sites, (2) monolayer adsorption where all identical adsorption sites are available, and (3) no interaction between adsorbates on adjacent adsorption sites. The Langmuir isotherm model is represented by eqn (3), and its linearized form is represented by eqn (4):

$$Q_e = \frac{C_e K_L Q_{max}}{1 + C_e K_L}, \quad (3)$$

$$\frac{C_e}{Q_e} = \frac{C_e}{Q_{max}} + \frac{1}{K_L Q_{max}}, \quad (4)$$

where Q_{max} (mg g^{-1}) represents the maximum adsorption capacity, C_e (mg L^{-1}) is the equilibrium concentration of the adsorbate, and K_L (L mg^{-1}) is the Langmuir adsorption constant related to adsorption energy.

The correlation of equilibrium concentrations with adsorption capacities was plotted at each temperature for all Ln ions. The results for La, Eu, and Lu as representative light, medium, and heavy lanthanides, respectively, are shown in Fig. 7(a)–(f), together with the Langmuir fittings. The fitting results of other Ln ions are shown in Fig. S5 and S6. All the corresponding parameters are listed in Table 1. The Langmuir eqn (3) was found to provide good non-linear regression with the determination coefficients (R^2) in the range of 0.984–0.992 for all Ln ions. Moreover, the linear regression based on eqn (4) exhibited a better fit to the Langmuir model, as indicated by the correlation coefficients (R) of 0.992–0.996. In contrast, when assuming multilayer adsorption on predominantly heterogeneous surfaces in a restricted range of adsorbate concentrations, the Freundlich isotherm model, which is empiri-

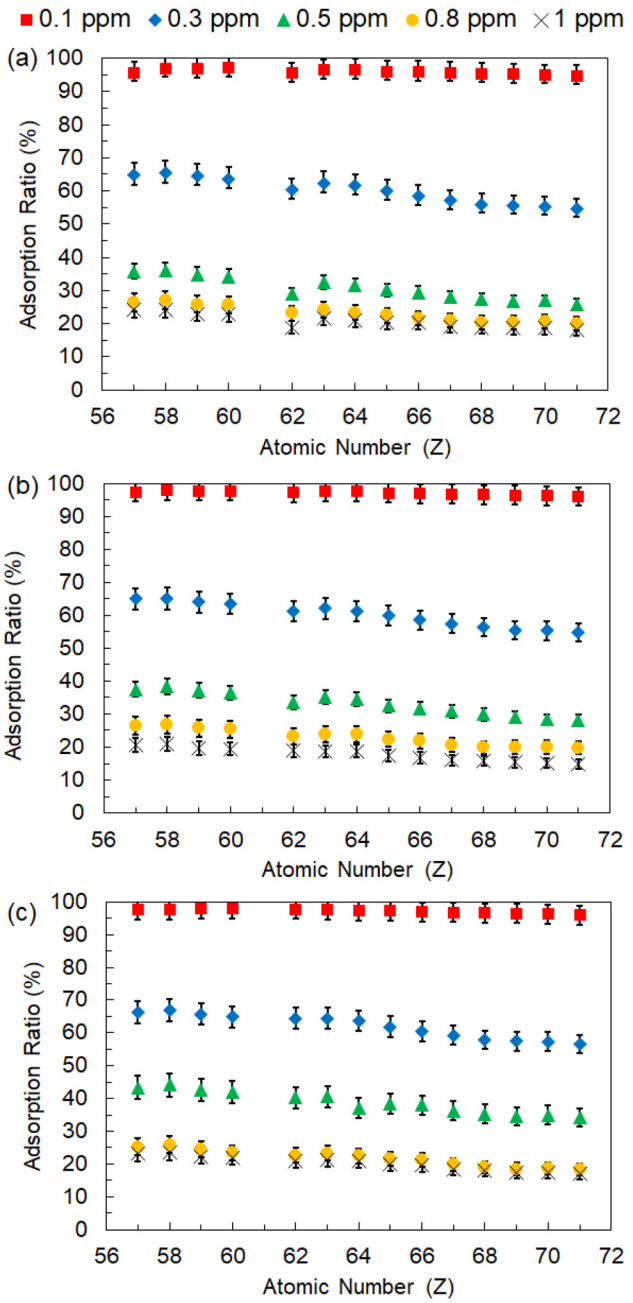

Fig. 6 Adsorption rates of all Ln ions (atomic numbers of 57 to 71 corresponding to La to Lu, respectively) on P-SiO_2-poly(DMAPS) at temperatures of (a) 50 °C, (b) 60 °C, and (c) 70 °C.

cal, can be applied. The Freundlich isotherm model is represented by eqn (5), as follows:

$$Q_e = K_F C_e^{\frac{1}{n}} \quad (5)$$

where C_e (mg L^{-1}) is the equilibrium concentration of the adsorbate and K_F $\left(\frac{mg^{\left(1-\frac{1}{n}\right)} L^{\left(\frac{1}{n}\right)}}{g}\right)$ and n are the Freundlich constants related to the adsorption capacity and adsorption intensity, respectively. The plots of Q_e *versus* C_e were found to have no significant fits to the Freundlich isotherm model (Fig. S7). Their R^2 values were within 0.5–0.8, which were lower than those in the case of the Langmuir isotherm model. The better fitting of the Langmuir isotherm model indicated that the poly(DMAPS) brushes possessed structurally homogeneous and energetically identical adsorption sites for Ln ions.

According to the Langmuir regression analysis, Q_{max} and K_L could be obtained for all Ln(III) ions, as listed in Table 1. The Q_{max} values for light Ln (La to Nd) were 0.02 mg g^{-1} or more, regardless of the temperature, but they decreased with increasing atomic numbers, reaching about 0.015–0.017 mg g^{-1} in the case of Lu. On the other hand, the effects of the Ln atomic numbers on K_L values showed different trends depending on the temperature. It was found that the K_L values at 50 °C were about 25–30 irrespective of the Ln atomic number, while for heavy Ln (Yb and Lu), the values increased with increasing temperature and Ln atomic number, exceeding about 1000 at 70 °C.

When we calculated the average Q_{max} values across all the lanthanides, Q_{max} could be estimated to be around 0.25 mg g^{-1} for single-elemental lanthanide ions. By dividing the number of moles of monomer units ($n_{monomoer}$) by the number of moles of La^{3+} (n_{La}) estimated from the Q_{max} value in 1 g of the polymer, the binding ratio could be determined as follows:

$$\text{Binding ratio} = \frac{n_{monomer}}{n_{La}} = \frac{\frac{Q_{max}}{M_w \text{ of La}}}{\frac{1\,\text{gram}}{M_w \text{ of monomer}}} = \frac{\frac{0.25\,\text{mg g}^{-1}}{138.9\,\text{g mol}^{-1} \times 1000\,\text{mg g}^{-1}}}{\frac{1\,\text{g}}{279.35\,\text{g mol}^{-1}}} \approx 2000. \quad (6)$$

Results suggested that La^{3+} interacts with approximately 2000 monomer units on the polymer brush, which is equivalent to one La^{3+} per around 42 polymer chains (with DP = 47). This simple estimation is unrealistic in terms of chemical coordination, but it explicitly demonstrates that only some moieties of the monomers on the polymer brush act as effective adsorption sites. Trivalent lanthanide ions are highly hydrated and require multidentate coordination sites to form stable complexes. In other words, multiple negatively charged sulfonates within the zwitterionic fragments must cooperatively occupy a single metal ion. As a result, many potential binding sites on the brush are not accessible. Given that the adsorption data fit the Langmuir isotherm model, the present Ln adsorption processes can be considered to occur not uniformly across the entire monomers but at discrete specific sites. Actually, the adsorption experiments using single-elemental solutions (La, Gd, Lu; each 1 ppm) showed that the adsorption ratios of each ion were larger than those in multi-elemental solutions even at the same concentrations (see Fig. S8).

The determination of thermodynamic parameters such as the standard enthalpy change ($\Delta H°$), standard entropy change ($\Delta S°$), and standard Gibbs free energy change ($\Delta G°$) is useful for elucidating the adsorption processes of Ln(III) on the poly

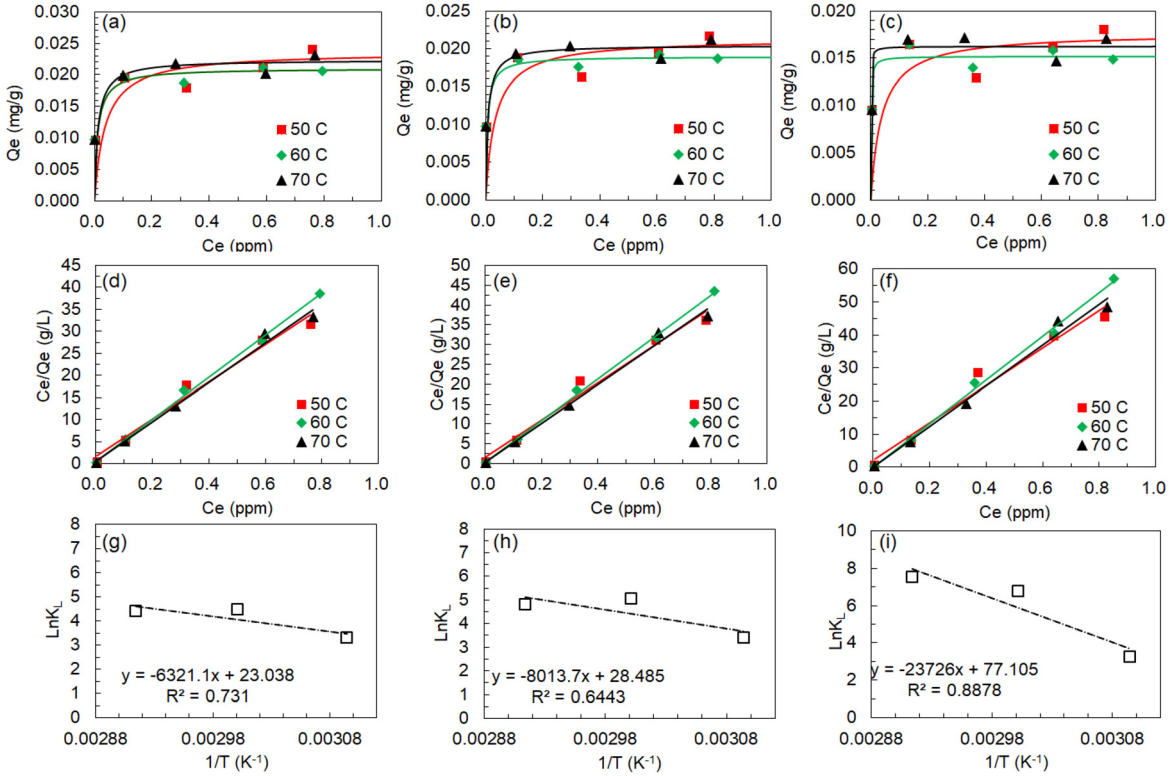

Fig. 7 Effects of initial concentrations on the adsorption capacities of (a) La(III), (b) Eu(III), and (c) Lu(III), as representative lanthanides, within 50 °C–70 °C. Corresponding Langmuir adsorption isotherm model fittings at 50 °C–70 °C (d, e, f) and van't Hoff plots (g, h, i).

Table 1 Determination coefficient (R^2) and correlation coefficient (R) of Langmuir regression analysis and the Q_{max} and K_L values obtained from the regression analysis

	Langmuir fitting			50 °C		60 °C		70 °C	
	Z	R^2	R	Q_{max}	K_L	Q_{max}	K_L	Q_{max}	K_L
La	57	0.991	0.995	0.0236 ± 0.0012	26.663 ± 2.310	0.0209 ± 0.0013	86.777 ± 15.175	0.0223 ± 0.0009	82.383 ± 16.153
Ce	58	0.992	0.996	0.0239 ± 0.0016	28.167 ± 5.167	0.0213 ± 0.0010	85.807 ± 20.442	0.0227 ± 0.0011	81.705 ± 21.987
Pr	59	0.992	0.996	0.0227 ± 0.0014	30.566 ± 5.554	0.0200 ± 0.0009	151.633 ± 18.060	0.0215 ± 0.0013	105.511 ± 14.726
Nd	60	0.986	0.993	0.0225 ± 0.0011	29.432 ± 3.632	0.0197 ± 0.0011	146.003 ± 24.694	0.0209 ± 0.0012	116.325 ± 19.995
Pm	61								
Sm	62	0.989	0.994	0.0189 ± 0.00105	35.986 ± 4.123	0.0189 ± 0.0008	80.0424 ± 12.057	0.0199 ± 0.0008	147.489 ± 10.042
Eu	63	0.991	0.995	0.0213 ± 0.00108	29.538 ± 3.701	0.0189 ± 0.0006	156.132 ± 14.070	0.0204 ± 0.0010	123.028 ± 11.514
Gd	64	0.987	0.994	0.0206 ± 0.00110	30.198 ± 4.015	0.0190 ± 0.0008	107.248 ± 15.669	0.0200 ± 0.0011	71.122 ± 22.846
Tb	65	0.989	0.995	0.0198 ± 0.00130	29.155 ± 3.445	0.0175 ± 0.0009	184.815 ± 17.425	0.0189 ± 0.001	161.871 ± 18.866
Dy	66	0.989	0.994	0.0195 ± 0.00109	26.811 ± 2.371	0.0170 ± 0.0011	266.459 ± 21.306	0.0186 ± 0.0008	161.996 ± 17.097
Ho	67	0.986	0.993	0.0186 ± 0.00150	28.159 ± 3.911	0.0162 ± 0.0009	811.291 ± 15.457	0.0175 ± 0.0009	274.578 ± 16.04
Er	68	0.984	0.992	0.0182 ± 0.00170	28.077 ± 3.788	0.0158 ± 0.0012	420.206 ± 16.706	0.0169 ± 0.0010	383.554 ± 19.961
Tm	69	0.983	0.992	0.0181 ± 0.00120	26.475 ± 2.015	0.0155 ± 0.0009	620.791 ± 21.456	0.0165 ± 0.0011	734.637 ± 13.114
Yb	70	0.986	0.993	0.0183 ± 0.00103	25.524 ± 1.956	0.0153 ± 0.0013	542.448 ± 13.238	0.0165 ± 0.0012	3278.541 ± 10.67
Lu	71	0.986	0.993	0.0176 ± 0.00104	26.034 ± 2.345	0.0151 ± 0.0008	869.013 ± 12.731	0.0162 ± 0.0010	1830.267 ± 20.283

(DMAPS) brush in detail. The $\Delta H°$, $\Delta S°$, and $\Delta G°$ values were estimated using the following equations:[43–46]

$$\ln K_L = -\frac{\Delta H°}{RT} + \frac{\Delta S°}{R}, \quad (7)$$

$$\Delta G° = \Delta H° - T\Delta S°, \quad (8)$$

where R is the universal gas constant (8.314 J mol^{-1} K^{-1}), K_L is the Langmuir constant, and T is the temperature. The $\Delta H°$ and $\Delta S°$ values were determined from the slope and intercept, respectively, of the plot of ln K_L *versus* $1/T$ (a van't Hoff plot) according to eqn (7), as shown in Fig. 7(g)–(i) and Fig. S9 for all Ln ions. The obtained $\Delta H°$ and $\Delta S°$ values are listed in Table 2, and their values are plotted against the Ln atomic numbers in Fig. S10. As a result, both $\Delta H°$ and $\Delta S°$ were

Table 2 Thermodynamic parameters of each Ln ion adsorbed onto P-SiO_2-poly(DMAPS)

	Z	$\Delta H°$ (kJ mol^{-1})	$\Delta S°$ (kJ mol^{-1} K^{-1})	$\Delta G°$ (T = 50 °C)	$\Delta G°$ (T = 60 °C)	$\Delta G°$ (T = 70 °C)
La	57	52.55 ± 3.3	0.1915 ± 0.010	−9.34 ± 0.03	−11.26 ± 0.13	−13.17 ± 0.23
Ce	58	49.61 ± 2.9	0.1827 ± 0.012	−9.46 ± 0.03	−11.29 ± 0.12	−13.11 ± 0.22
Pr	59	57.99 ± 3.1	0.2105 ± 0.011	−10.03 ± 0.03	−12.13 ± 0.l1	−14.23 ± 0.19
Nd	60	64.17 ± 2.8	0.2291 ± 0.009	−9.86 ± 0.03	−12.15 ± 0.13	−14.44 ± 0.20
Pm	61					
Sm	62	65.09 ± 3.5	0.2314 ± 0.011	−9.69 ± 0.02	−12.00 ± 0.14	−14.31 ± 0.19
Eu	63	66.62 + 3.0	0.2368 + 0.009	−9.90 + 0.03	−12.27 + 0.15	−14.64 + 0.20
Gd	64	40.24 ± 2.5	0.1551 ± 0.012	−9.87 ± 0.04	−11.42 ± 0.12	−12.97 ± 0.21
Tb	65	79.90 ± 2.9	0.2779 ± 0.013	−9.89 ± 0.03	−12.67 ± 0.l l	−15.45 ± 0.22
Dy	66	84.17 ± 2.8	0.2915 ± 0.013	−9.87 ± 0.02	−12.94 ± 0.l 3	−15.85 ± 0.21
Ho	67	106.99 ± 3.1	0.3647 ± 0.014	−10.87 ± 0.03	−14.51 ± 0.14	−18.16 ± 0.20
Er	68	121.77 + 3.2	0.4082 + 0.010	−10.14 + 0.04	−14.22 + 0.15	−18.30 + 0.25
Tm	69	154.51 ± 3.0	0.5092 ± 0.010	−10.06 ± 0.02	−15.15 ± 0.11	−20.24 ± 0.23
Yb	70	224.33 ± 2.9	0.7226 ± 0.010	−9.18 + 0.03	−16.40 + 0.l 0	−23.63 + 0.18
Lu	71	197.25 + 2.8	0.6410 + 0.012	−9.89 + 0.02	−16.30 + 0.13	−22.72 + 0.20

found to take positive values for all Ln and increase with increasing Ln atomic numbers. The positive $\Delta H°$ values indicated the endothermic feature of the adsorption of Ln(III) ions onto P-SiO_2-poly(DMAPS). Previous studies indicate that $\Delta H°$ values become 20 kJ mol^{-1} or less for physisorption, invoking weak electrostatic interactions between adsorbate (Ln ions) and adsorbent (surfaces), and 80–200 kJ mol^{-1} for chemisorption, invoking adsorbate–adsorbent chemical bond formation.[46,47] Thus, the large $\Delta H°$ values (50–220 kJ mol^{-1}) obtained in the present study indicated that the chemisorption of Ln(III) ions with the functional moieties of P-SiO_2-poly (DMAPS) is the dominant pròcess.

In addition, the positive $\Delta S°$ values reflect an increase in the randomness (degrees of freedom) at the solid–liquid interface during Ln(III) adsorption, indicating an entropy-driven adsorption process. It has been established that an increase in the $\Delta S°$ of the system, caused by the adsorption of metal ions from the solution on the adsorbent surface, is associated with the exchange and release of water molecules in the hydration shell of metal ions with those around the adsorption sites.[48,49] As shown in Fig. S10, P-SiO_2-poly(DMAPS) was found to obtain larger positive $\Delta S°$ values for heavy Ln ions. The almost plateau-like $\Delta S°$ values of about 200 J mol^{-1} K^{-1} for light and middle Ln ions (La to Gd) were drastically enhanced with increasing Ln atomic numbers from Gd to Lu, reaching a maximum of about 700 J mol^{-1} K^{-1}. The greater hydration stabilities of heavy Ln ions with smaller ionic radii and higher charge densities are responsible for the increase in the energy required for dehydration.[50–52] Thus, when Ln(III) ions interacted with P-SiO_2-poly(DMAPS) surfaces, accompanied by dehydration, the heavy Ln ions could lead to a greater degree of disorder or randomness in the system, resulting in higher $\Delta S°$ values.

The $\Delta G°$ of Ln(III) adsorption can be determined using eqn (7). The $\Delta G°$ values obtained at each temperature are listed in Table 2. All $\Delta G°$ values were negative, suggesting that the Ln (III) adsorption processes on the poly(DMAPS) brush surface occurred spontaneously. Notably, at 50 °C, irrespective of the Ln(III) ions, $\Delta G°$ values were almost constant between −10 kJ mol^{-1} and −9 kJ mol^{-1}, while they became more negative at higher temperatures, falling below −20 kJ mol^{-1} for heavy Ln ions at 70 °C.

The characteristics of equilibrium adsorption can be evaluated using a separation factor (equilibrium parameter), R_L, which is a dimensionless constant calculated using eqn (9):[53–56]

$$R_L = \frac{1}{1 + K_L C_0}, \quad (9)$$

where C_0 and K_L represent the initial concentration of the adsorbate and the Langmuir constant, respectively. The R_L value defines whether the adsorption process is favorable ($0 < R_L < 1$), unfavorable ($R_L > 1$), linear ($R_L = 1$), or irreversible ($R_L = 0$). As shown in Fig. 8, all R_L values were less than unity at all initial Ln concentrations (C_0) and decreased with increasing C_0. Moreover, the R_L values were confirmed to increase in the order of atomic numbers above 60 °C (La > Nd > Dy > Lu) or in the order of larger ionic radii. The R_L values for Ln species were larger at 50 °C than those at above 60 °C, and no differences in R_L values were observed. Such differences in the temperature dependence between 50 °C and above 60 °C were consistent with the trends in $\Delta G°$, indicating that the adsorption of Ln(III) ions on P-SiO_2-poly(DMAPS) was favorable at higher temperature states.

In general, an adsorption system with a smaller R_L value tends to take a larger Q_{max} value, but in the present P-SiO_2-poly (DMAPS) system, the Q_{max} values for light Ln ions became larger despite the larger R_L and smaller negative $\Delta G°$ values. The reverse correlation between the R_L and Q_{max} values could be caused by the hydration states of Ln(III). Heavy Ln ions with greater hydration energies have a strong affinity to the hydrophilic P-SiO_2-poly(DMAPS) above T_c and can approach the brush surroundings more spontaneously, which lowers the magnitude of $\Delta G°$. However, since adsorption is based on an entropy-driven process, there is extensive disordering and randomness in the entire adsorption system due to the dehydration and water exchange of the heavy Ln ions. This hinders the efficient chemical bonding between heavy Ln ions and the functional moieties of P-SiO_2-poly(DMAPS). On the other hand, light Ln ions show

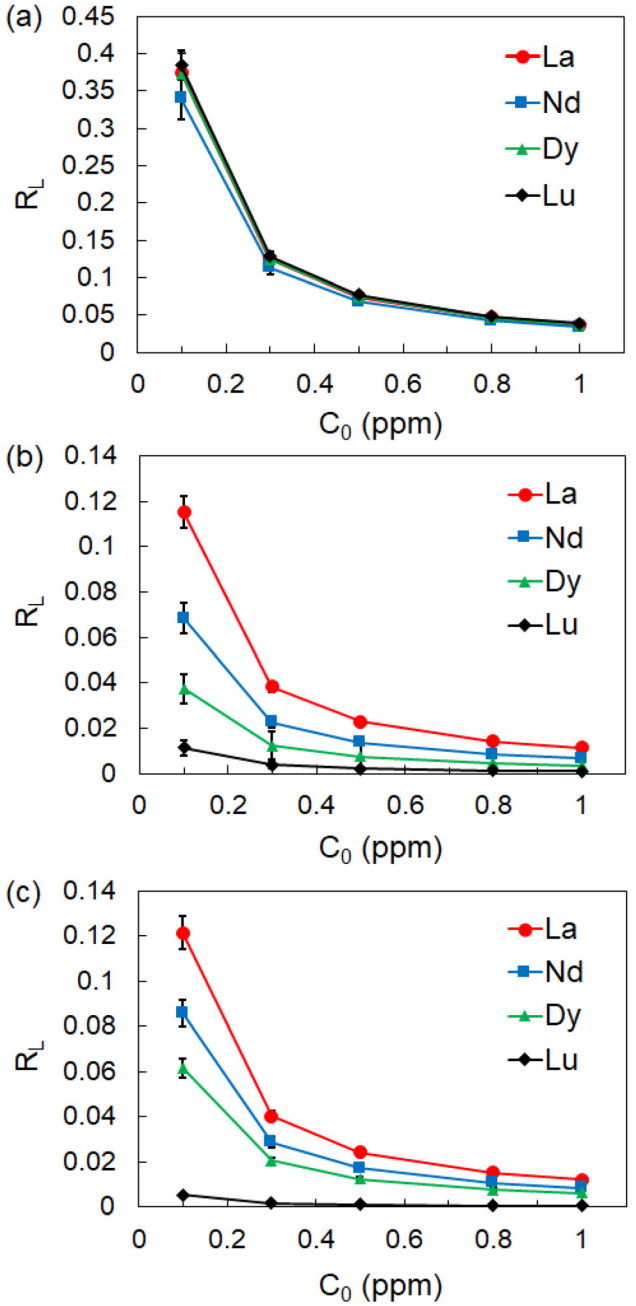

Fig. 8 Dependence of R_L constant on the initial concentration of Ln ions at (a) 50 °C, (b) 60 °C, and (c) 70 °C.

energetically unfavorable features when compared with heavy Ln ions, but they can be easily dehydrated. Shielding effects are also reduced due to the absence of water molecules, allowing them to chemically interact with the P-SiO_2-poly(DMAPS) surfaces with smaller entropy changes. It is also possible that the Ln(III) adsorption on P-SiO_2-poly(DMAPS) proceeds *via* a competitive reaction between dehydration and chemisorption and that the Q_{max} values for light Ln ions with lower $\Delta G°$ values become higher than those for heavy Ln ions having higher $\Delta G°$ values at equilibrium states.

3.4. Desorption of lanthanide ions from the poly(DMAPS) brush

To realize the efficient detachment of Ln ions adsorbed onto P-SiO_2-poly(DMAPS), desorption experiments were performed on Ln ions using the brushes that adsorbed 100% of Ln ions in desorption solutions containing HNO_3, HCl, Dien, and EDTA at below the T_c (5 °C) of poly(DMAPS). Fig. 9 shows the desorption ratios of all Ln ions treated in the acidic solutions of HNO_3 and HCl. In both the solutions, it was found that the desorption ratios reached almost 100% at highly acidic concentrations above 0.1 M, but the desorption of Ln ions from the brushes was less likely to proceed under low acid concentrations, with no desorption occurring below the acidic concentration of 0.001 M. These results indicated that Ln(III) adsorbed on P-SiO_2-poly(DMAPS) could be desorbed under highly acidic environments due to competitive binding of H^+ to the sulfonate groups, which disrupts the lanthanide-sulfonate interactions and promoting the detachment of Ln(III) into the aqueous phase.

The desorption performance of Ln ions was compared with aqueous solutions containing Dien and EDTA. As shown in Fig. 10(a), when desorption was performed in an EDTA solution of 0.01 M, almost 100% desorption of all Ln ions took place, which was higher than that achieved (about 80%) *via* acidic treatment under the same concentration. This superior desorption ability of EDTA is caused by the formation of water-soluble Ln chelate complexes through the lone pair of electrons on the nitrogen and oxygen atoms of EDTA. On the other hand, treatment with Dien could not facilitate the desorption of Ln ions, despite Dien having the potential similar to that of EDTA to coordinate with Ln ions. This 0% desorption might be because Dien, being a small N-donor molecule, might not offer enough coordination sites for complexation with Ln ions desorbed from the P-SiO_2-poly(DMAPS) in aqueous solutions.

The effects of EDTA concentrations on the desorption ratios of Ln ions were examined to optimize the detachment conditions from P-SiO_2-poly(DMAPS). The results are shown in Fig. 10(b). We found that the equilibrium was shifted to the formation of Ln(III)-EDTA complexes upon adding EDTA, and the desorption ratios of all Ln ions could reach 100% at 1×10^{-3} M EDTA. Herein, it is noteworthy that a reduction in the desorption ratios of Ln ions was observed at EDTA concentrations above or below 1×10^{-3} M. In the case of higher EDTA concentrations (above 1×10^{-3} M), an excess amount of EDTA may bind to P-SiO_2-poly(DMAPS) and affect the equilibrium, potentially leading to Ln(III) desorption from the polymer brushes. Meanwhile, lowering the EDTA concentration led to varying desorption tendencies. At the concentration of 1×10^{-4} M, the desorption ratios for all Ln ions remained at 65%, most likely due to insufficient Ln(III)-EDTA complex formation in aqueous solutions. As the EDTA concentration was reduced to 1×10^{-5} M, it was found that the desorption ratios of gadolinium (Z = 64) and higher atomic number lanthanides were consistent with the case of 1×10^{-4} M, but their desorption ratios were linearly suppressed to a minimum of 9.2% from Gd to La (lighter lanthanide side). This fact indicates that the

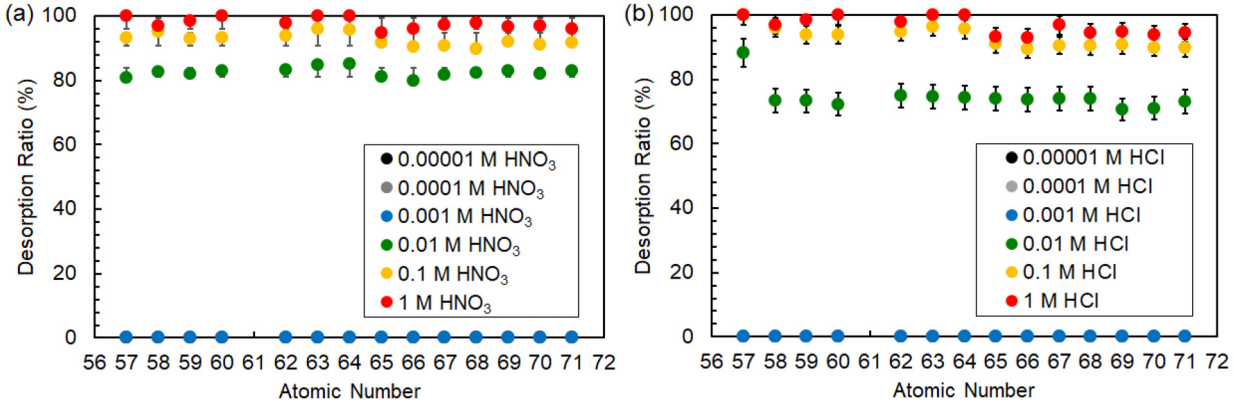

Fig. 9 Desorption rates of all Ln ions from P-SiO_2-poly(DMAPS) that adsorbed 100% of Ln ions by treatment with (a) HNO_3 and (b) HCl solutions.

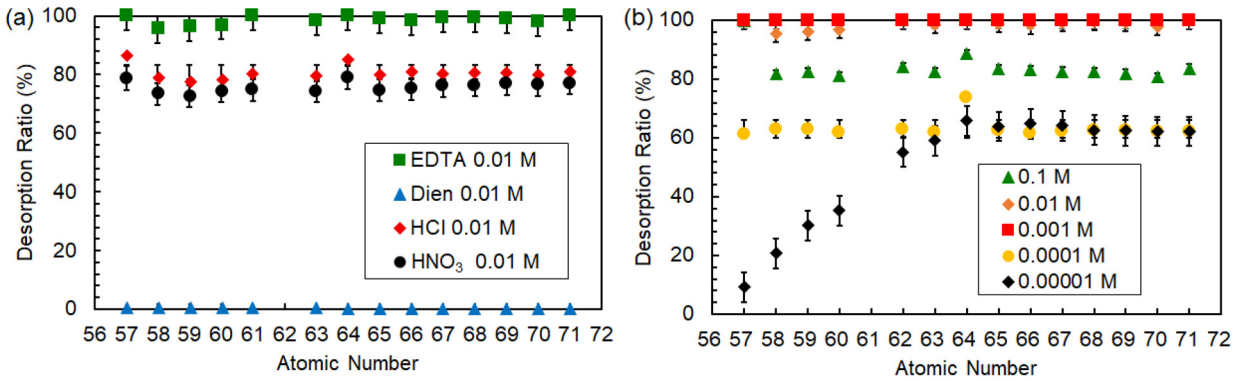

Fig. 10 Desorption rates of all Ln ions treated with (a) various types of eluents, such as HNO_3, HCl, EDTA, and Dien, and (b) various concentrations of EDTA.

energetically favorable heavy Ln ions could preferentially coordinate with EDTA in aqueous solutions containing insufficient EDTA, promoting the efficient detachment of heavy Ln ions rather than light Ln ions. As a result, controlling EDTA concentration below T_c can smoothly and selectively recover lanthanide ions which are efficiently desorbed through preferential complexation with EDTA, while light lanthanide ions remain associated with the brush.

3.5. Evaluation of the reusability of the poly(DMAPS) brush

To elucidate the reusability of the P-SiO_2-poly(DMAPS), repetitive adsorption tests of Ln ions were conducted. The P-SiO_2-poly(DMAPS) was reacted with $Ln(NO_3)_3$ solutions (Ln = La to Lu, each concentration = 1 ppm) at 50 °C (above UCST), and the adsorption ratios of Ln ions were determined from the Ln concentration changes based on ICP-MS measurements. After all Ln ions were detached completely from the Ln-adsorbed solid brush matrixes using 0.01 M EDTA solution, the Ln adsorption experiments were carried out again. The results are shown in Fig. 11. It was found that P-SiO_2-poly(DMAPS) exhibited a maximum Ln adsorption percentage of approximately 25% under a high Ln concentration environment (1 ppm), and the dependence of the adsorption percentages on the Ln atomic number showed the same trend regardless of the number of repetitive operations (three times). The errors generated from the adsorption process were less than ±2%, which meant negligible effects of solution volume changes, but those from the desorption processes reached a maximum of approximately ±10%.

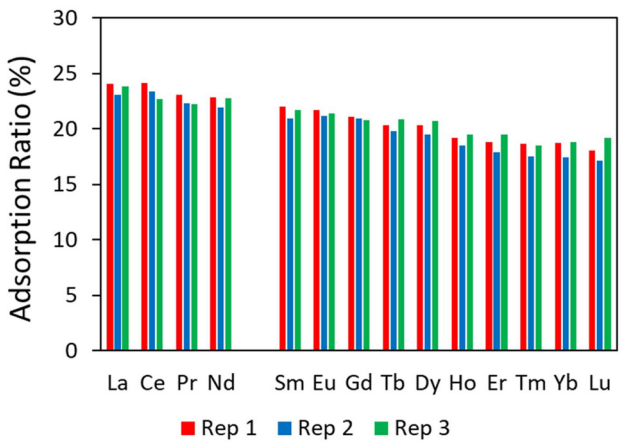

Fig. 11 Reusability of the poly(DMAPS) brush matrixes for Ln adsorption (initial Ln = 1 ppm).

Their errors are reflected in the plots in Fig. 6–10. The relatively large errors in desorption could be caused by residual solutions within the P-SiO_2-poly(DMAPS). To confirm the effect of residual solution, P-SiO_2-poly(DMAPS) (100 mg) was recovered after removing the supernatant used in the adsorption test by centrifugation. After that, 10 μL of aqueous solution was gently dropped into a PP tube containing P-SiO_2-poly(DMAPS). Upon reaching 50 μL, the added aqueous solution was found to be leached out onto the exterior of the P-SiO_2-poly(DMAPS) surface, suggesting that 50 μL of residual solution within the polymer brush caused the desorption errors. From these results, it was concluded that the P-SiO_2-poly(DMAPS) matrix has superior reusability for Ln adsorption–desorption within the above-mentioned margin of error.

4. Conclusions

A novel zwitterionic polymer-grafted porous silica particle (P-SiO_2-poly(DMAPS)) was successfully fabricated *via* SI-ATRP and characterized by various analytical methods. Its T_c in aqueous solutions shifted depending on the valence numbers and types of metal ions and Ln(III) concentrations, leading to the development of optimal adsorption–desorption experimental conditions. The P-SiO_2-poly(DMAPS) could adsorb 100% of Ln(III) from aqueous solutions. The equilibrium concentration dependence of the adsorption capacities for all Ln ions was examined at temperatures in the range of 50 °C–70 °C. The isothermal curves for Ln adsorption on P-SiO_2-poly(DMAPS) exhibited good non-linear and linear regressions according to a single-component Langmuir isotherm model, but no significant regression was observed in the Freundlich isotherm model. The maximum adsorption capacities (Q_{max}) of light Ln (La to Nd) were determined to be 0.02 mg g^{-1} or more, regardless of temperature, and decreased with increasing atomic numbers to about 0.015–0.017 mg g^{-1} for heavy Ln. From the thermodynamic parameters of $\Delta H°$, $\Delta S°$, and $\Delta G°$ estimated from the Langmuir isotherm model fittings, the adsorption processes of all Ln ions on P-SiO_2-poly(DMAPS) were found to be dominantly entropy-driven and spontaneous chemisorption. Since the increase in the Ln atomic numbers caused negative increases in the $\Delta G°$ values and decreases in the Q_{max} values, the adsorption of Ln ions on P-SiO_2-poly(DMAPS) would be controlled by the competitive reactions between dehydration and chemisorption. All Ln ions adsorbed on P-SiO_2-poly(DMAPS) were completely desorbed in an EDTA solution of 1×10^{-3} M below the T_c value, and lower EDTA concentrations (1×10^{-5} M or less) enabled the selective desorption of heavy Ln ions. This separation process using P-SiO_2-poly(DMAPS) is a green and effective methodology for the recovery of target Ln metal ions from environmental and industrial wastewaters.

Author contributions

Tommy Suhartono Wijaya Tan: investigation, methodology, validation, writing – original draft. Naokazu Idota: investigation, methodology, validation, writing – review & editing. Takehiko Tsukahara: conceptualization, methodology, validation, writing – review & editing, supervision, funding acquisition, resources.

Conflicts of interest

There are no conflicts to declare.

Data availability

The data that support the findings of this study are available within the article and its supplementary information (SI). Supplementary information is available. See DOI: https://doi.org/10.1039/d5lp00239g.

Acknowledgements

This work was supported by the Secretariat of the Nuclear Regulation Authority, Japan, and JAEA Nuclear Energy S&T and Human Resource Development. Project grant number: JPJA22F22717857.

References

1 R. Ganguli and D. R. Cook, Rare earths: A review of the landscape, *MRS Energy Sustain.*, 2018, **5**, 1–16, DOI: 10.1557/mre.2018.7.
2 V. Balaram, Rare earth elements: A review of applications, occurrence, exploration, analysis, recycling, and environmental impact, *Geosci. Front.*, 2019, **110**, 1285–1303, DOI: 10.1016/j.gsf.2018.12.005.
3 W. Weng, A. Biesiekierski, Y. Li, M. Dargusch and C. Wen, A review of the physiological impact of rare earth elements and their uses in biomedical Mg alloys, *Acta Biomater.*, 2021, **130**, 80–97, DOI: 10.1016/j.actbio.2021.06.004.
4 P. P. Dagwar, S. S. Iqbal and D. Dutta, Sustainable recovery of rare Earth elements from industrial waste: A path to circular economy and environmental health, *Waste Manag. Bull.*, 2025, **3**, 373–390, DOI: 10.1016/j.wmb.2025.02.004.
5 B. Liang, J. Gu, X. Zeng, W. Yuan, M. Rao, B. Xiao and H. Hu, A Review of the Occurrence and Recovery of Rare Earth Elements from Electronic Waste, *Molecules*, 2024, **29**, 4624, DOI: 10.3390/molecules29194624.
6 S. Praneeth, A. K. Sakr, M. Dardona, C. M. Tummala, P. K. Roy and T. M. Dittrich, Selective separation and recovery of rare-earth elements (REEs) from acidic solutions and coal fly ash leachate by novel TODGA-Impregnated organosilica media, *Chem. Eng. J.*, 2024, **500**, 156849, DOI: 10.1016/j.cej.2024.156849.
7 B.-M. Jun, H.-H. Kim, H. Rho, J. Seo, J.-W. Jeon, S.-N. Nam, H. M. Park and Y. Yoon, Recovery of rare-earth and radioactive elements from contaminated water through precipi-

tation: A review, *Chem. Eng. J.*, 2023, **475**, 146222, DOI: 10.1016/j.cej.2023.146222.

8 P. Banerjee, S. A. Ansari, P. K. Mohapatra, R. J. M. Egberink, S. Ramasubramanium, C. B. Patil, J. Huskens and W. Verboom, Highly Efficient Europium(III) Uptake with an Extraction Chromatographic Resin Containing a Unique Multiple Diglycolamide Ligand with a Tetraaza-12-crown-4 Scaffold, *Ind. Eng. Chem. Res.*, 2021, **60**, 2613–2624, DOI: 10.1021/acs.iecr.1c00186.

9 K. De Jesus, R. Rodriguez, D. L. Baek, R. V. Fox, S. Pashikanti and K. Sharma, Extraction of lanthanides and actinides present in spent nuclear fuel and in electronic waste, *J. Mol. Liq.*, 2021, **336**, 116006, DOI: 10.1016/j.molliq.2021.116006.

10 S. A. Ansari, P. Pathak, P. K. Mohapatra and V. K. Manchanda, Chemistry of Diglycolamides: Promising Extractants for Actinide Partitioning, *Chem. Rev.*, 2012, **112**, 1751–1772, DOI: 10.1021/cr200002f.

11 A. G. Baldwin, A. S. Ivanov, N. J. Williams, R. J. Ellis, B. A. Moyer, V. S. Bryantsev and J. C. Shafer, Outer-sphere water clusters tune the lanthanide selectivity of diglycolamides, *ACS Cent. Sci.*, 2018, **4**, 739–747, DOI: 10.1021/acscentsci.8b00223.

12 R. Paz, N. K. Gupta, H. Viltres, C. Leyva, A. Romero-Galarza, S. Srinivasan and A. R. Rajabzadeh, Lanthanides adsorption on metal-organic framework: Experimental insight and spectroscopic evidence, *Sep. Purif. Technol.*, 2022, **298**, 121606, DOI: 10.1016/j.seppur.2022.121606.

13 M. Otaki, T. Suominen, S. Hietala and R. T. Koivula, Intra-lanthanide separation performance of DOTP: Solid-phase extraction and selective precipitation studies, *Sep. Purif. Technol.*, 2025, **354**, 129082, DOI: 10.1016/j.seppur.2024.129082.

14 J. Florek, D. Larivière, H. Kählig, S. L. Fiorilli, B. Onida, F.-G. Fontaine and F. Kleitz, Understanding Selectivity of Mesoporous Silica-Grafted Diglycolamide-Type Ligands in the Solid-Phase Extraction of Rare Earths, *ACS Appl. Mater. Interfaces*, 2020, **12**, 57003–57016, DOI: 10.1021/acsami.0c16282.

15 Y. Nutthon and T. Tsukahara, Temperature Swing Mutual Separation of Lanthanide Ions Using Thermoresponsive Polymer Brushes, *Chem. Lett.*, 2018, **47**, 1051–1054, DOI: 10.1246/cl.180447.

16 K. C. Park, N. Idota and T. Tsukahara, Synthesis of NIPAAm-based polymer-grafted silica beads by surface-initiated ATRP using Me4Cyclam ligands and the thermo-responsive behaviors for lanthanide(III) ions, *React. Funct. Polym.*, 2014, **79**, 36–46, DOI: 10.1016/j.reactfunctpolym.2014.03.011.

17 R. B. Gujar, S. A. Ansari, P. K. Mohapatra and W. Verboom, Highly Promising Method for the Decontamination of Europium from Americium Using an Extraction Chromatography Resin Containing a Tripodal Diglycolamide and SO3Ph-BTP as Eluent, *Ind. Eng. Chem. Res.*, 2023, **62**, 15157–15165, DOI: 10.1021/acs.iecr.3c01923.

18 K.-Q. Ma, F. Zhang, H. Yan, C.-F. Zhang, Y. Liu, M. Gu, C.-T. Yang, S. Hu and L. Shi, Separation of minor actinides from highly acidic solutions using diglycolamide modified mesoporous silica synthesized via a novel "ring-opening click" reaction, *Chem. Eng. J.*, 2022, **436**, 135213, DOI: 10.1016/j.cej.2022.135213.

19 H. Hoshi, Y.-Z. Wei, M. Kumagai, T. Asakura and Y. Morita, Group separation of trivalent minor actinides and lanthanides by TODGA extraction chromatography for radioactive waste management, *J. Alloys Compd.*, 2004, **374**, 451–455, DOI: 10.1016/j.jallcom.2024.177072.

20 S. Y. Ning, X. P. Wang, Q. Zou, W. Q. Shi, F. D. Tang, L. F. He and Y. Z. Wei, Direct separation of minor actinides from high level liquid waste by Me2-CA-BTP/SiO_2-P adsorbent, *Sci. Rep.*, 2017, **7**, 14679, DOI: 10.1038/s41598-017-14758-2.

21 S. A. Ansari and P. K. Mohapatra, A review on solid phase extraction of actinides and lanthanides with amide based extractants, *J. Chromatogr. A*, 2017, **1499**, 1–20, DOI: 10.1016/j.chroma.2017.03.035.

22 Y. Xie, L. Yu, L. Chen, C. Chen, L. Wang, F. Liu, Y. Liao, P. Zhang, T. Chen, Y. Yuan, Y. Lu, B. Huang, H. Yang, S. Wang, S. Wang, L. Ma, F. Luo, Y. Liu, B. Hu, H. Wang, D. Pan, W. Zhu, N. Wang, Z. Wang, L. Mao, S. Ma and X. Wang, Recent progress of radionuclides separation by porous materials, *Sci. China: Chem.*, 2024, **67**, 3515–3577, DOI: 10.1007/s11426-024-2218-8.

23 J. Liu, Y. Ma, T. Xu and G. Shao, Preparation of zwitterionic hybrid polymer and its application for the removal of heavy metal ions from water, *J. Hazard. Mater.*, 2010, **178**, 1021–1029, DOI: 10.1016/j.jhazmat.2010.02.041.

24 M.-M. Zaharia, F. Bucatariu, A.-L. Vasiliu and M. Mihai, Versatile Zwitterionic Beads for Heavy Metal Ion Removal from Aqueous Media and Soils by Sorption and Catalysis Processes, *ACS Appl. Polym. Mater.*, 2023, **5**, 8183–8193, DOI: 10.1021/acsapm.3c01375.

25 E. O. Ningrum, T. Gotoh, W. Ciptonugroho, A. D. Karisma, E. Agustiani, Z. M. Safitri and M. A. Dzaky, Novel Thermosensitive-co-Zwitterionic Sulfobetaine Gels for Metal Ion Removal: Synthesis and Characterization, *Gels*, 2021, **7**, 273, DOI: 10.3390/gels7040273.

26 N. Chowdhury, Solaiman, C. K. Roy, S. H. Firoz, T. Foyez and A. B. Imran, Role of Ionic Moieties in Hydrogel Networks to Remove Heavy Metal Ions from Water, *ACS Omega*, 2021, **6**, 836–844 https://pubs.acs.org/doi/10.1021/acsomega.0c05411.

27 Q. He, Y. Qiao, C. M. Jimenez, R. Hackler, A. B. F. Martinson, W. Chen and M. V. Tirrell, Ion Specificity Influences on the Structure of Zwitterionic Brushes, *Macromolecules*, 2023, **56**, 1945–1953, DOI: 10.1021/acs.macromol.2c02029.

28 E. A. Q. Mondarte, Y. Shi, X. Q. Koh, X. Feng, D. Daniel, X.-X. Zhang and J. Yu, Unveiling the Layered Structure of Sulfobetaine Polymer Brushes through Bimodal Atomic Force Microscopy, *Macromolecules*, 2023, **56**, 5001–5009, DOI: 10.1021/acs.macromol.3c00721.

29 J. de Grooth, W. Ogieglo, W. M. de Vos, M. Gironès, K. Nijmeijer and N. E. Benes, Swelling dynamics of zwitterionic copolymers: The effects of concentration and type of anion and cation, *Eur. Polym. J.*, 2014, **55**, 57–65, DOI: 10.1016/j.eurpolymj.2014.03.021.

30 E. O. Ningrum, S. Sakohara and T. Gotoh, Suprapto and N. Humaidah, Correlating properties between sulfobetaine hydrogels and polymers with different carbon spacer lengths, *Polymer*, 2020, **186**, 122013, DOI: 10.1016/j.polymer.2019.122013.

31 E. O. Ningrum, Y. Murakami, Y. Ohfuka, T. Gotoh and S. Sakohara, Investigation of ion adsorption properties of sulfobetaine gel and relationship with its swelling behavior, *Polymer*, 2014, **55**, 5189–5197, DOI: 10.1016/j.polymer.2014.08.042.

32 P. L. Nostro and B. W. Ninham, Hofmeister Phenomena: An Update on Ion Specificity in Biology, *Chem. Rev.*, 2012, **112**, 2286–2322, DOI: 10.1021/cr200271j.

33 R. Farina, N. Laugel, J. Yu and M. Tirrell, Reversible Adhesion with Polyelectrolyte Brushes Tailored via the Uptake and Release of Trivalent Lanthanum Ions, *J. Phys. Chem. C*, 2015, **119**, 14805–14814, DOI: 10.1021/acs.jpcc.5b02121.

34 Q.-H. Hao, H.-Y. Qian, M.-L. Chao, H.-Y. Zhang, H.-G. Tan and B. Miao, A Systematic Study on Trivalent Salt Cationic Specificity through Polyelectrolyte Brushes, *Macromolecules*, 2025, **58**, 4082–4093, DOI: 10.1021/acs.macromol.4c02664.

35 J. Yu, N. E. Jackson, X. Xu, Y. Morgenstern, Y. Kaufman, M. Ruths, J. J. de Pablo and M. Tirrell, Multivalent counterions diminish the lubricity of polyelectrolyte brushes, *Science*, 2018, **360**, 1434–1438, DOI: 10.1126/science.aar5877.

36 Y. Higaki, M. Kobayashi and A. Takahara, Hydration State Variation of Polyzwitterion Brushes through Interplay with Ions, *Langmuir*, 2020, **36**, 9015–9024, DOI: 10.1021/acs.langmuir.0c01672.

37 K. K. Sharker, Y. Ohara, Y. Shigeta, S. Ozoe and S. Yusa, Upper Critical Solution Temperature (UCST) Behavior of Polystyrene-Based Polyampholytes in Aqueous Solution, *Polymers*, 2018, **11**, 265, DOI: 10.3390/polym11020265.

38 J. Niskanena and H. Tenhu, How to manipulate the upper critical solution temperature (UCST)?, *Polym. Chem.*, 2017, **8**, 220, DOI: 10.1039/C6PY01612J.

39 N. Kato, H. Hashizume, Y. Sakai and T. Uyehara, Effect of Alkali Metal Halides on the Upper Critical Solution Temperature of Poly(N-acetylacrylamide) in Ethanol-Water System, *Anal. Sci.*, 2001, **17**, i1133–i1136, DOI: 10.14891/analscisp.17icas.0.i1133.0.

40 A. Smerigan, S. Biswas, F. D. Vila, J. Hong, J. Perez-Aguilar, A. S. Hoffman, L. Greenlee, R. B. Getman and S. R. Bare, Aqueous Structure of Lanthanide–EDTA Coordination Complexes Determined by a Combined DFT/EXAFS Approach, *Inorg. Chem.*, 2023, **62**, 14523–14532, DOI: 10.1021/acs.inorgchem.3c01334.

41 K. L. Nash, D. Brigham, T. C. Shehee and A. Martin, The kinetics of lanthanide complexation by EDTA and DTPA in lactate media, *Dalton Trans.*, 2012, **41**, 14547, DOI: 10.1039/C2DT31851B.

42 J.-C. Bollinger, K. H. Chu, L. Mouni and S. Salvestrini, Discussion on "Design of acid-geopolymers based on clays by-products for methylene blue removal from wastewater" [Appl. Clay Sci., 2023, 245, 107126], *Appl. Clay Sci.*, 2024, **254**, 107375, DOI: 10.1016/j.clay.2024.107375.

43 Y. Zhang, N. Idota and T. Tsukahara, Surface-functionalized polydimethylsiloxane sponges for facile and selective recovery of molybdenum from aqueous/acidic solutions, *J. Hazard. Mater.*, 2025, **488**, 137485, DOI: 10.1016/j.jhazmat.2025.137485.

44 Y. Liu, Is the Free Energy Change of Adsorption Correctly Calculated?, *J. Chem. Eng. Data*, 2009, **54**, 1981–1985, DOI: 10.1021/je800661q.

45 W. Kong, Q. Li, J. Liu, X. Li, L. Zhao, Y. Su, Q. Yue and B. Gao, Adsorption behavior and mechanism of heavy metal ions by chicken feather protein-based semi-interpenetrating polymer networks super absorbent resin, *RSC Adv.*, 2016, **6**, 83234, DOI: 10.1039/C6RA18180E.

46 B. N. Huda, E. T. Wahyuni, Y. Kamiya and M. Mudasir, Kinetic and thermodynamic study on adsorption of lead(II) ions in water over dithizone-immobilized coal bottom ash, *Mater. Chem. Phys.*, 2022, **282**, 126005, DOI: 10.1016/j.matchemphys.2022.126005.

47 R. Ejima, M. Nakahata, Y. Kamon and A. Hashidzume, Synthesis and Metal Ion Adsorption Properties of a Dense Triazole Polymer Carrying Cysteine Residues, *J. Polym. Sci.*, 2025, **63**, 1570–1579, DOI: 10.1002/pol.20240752.

48 N. Ünlü and M. Ersoz, Adsorption characteristics of heavy metal ions onto a low cost biopolymeric sorbent from aqueous solutions, *J. Hazard. Mater.*, 2006, **136**, 272–280, DOI: 10.1016/j.jhazmat.2005.12.013.

49 O. A. Alnasra, F. I. Khalili and F. A. Alhnafat, Enhanced removal of Pb(II), Zn(II) and Cd(II) ions by insolubilized humic acid: Characterization and sorption behaviors, *Desalin. Water Treat.*, 2024, **320**, 100604, DOI: 10.1016/j.dwt.2024.100604.

50 A. G. Baldwin, A. S. Ivanov, N. J. Williams, R. J. Ellis, B. A. Moyer, V. S. Bryantsev and J. C. Shafer, Outer-Sphere Water Clusters Tune the Lanthanide Selectivity of Diglycolamides, *ACS Cent. Sci.*, 2018, **4**, 739–747, DOI: 10.1021/acscentsci.8b00223.

51 P. D'Angelo, A. Zitolo, V. Migliorati, G. Chillemi, M. Duvail, P. Vitorge, S. Abadie and R. Spezia, Revised Ionic Radii of Lanthanoid(III) Ions in Aqueous Solution, *Inorg. Chem.*, 2011, **50**, 4572–4579, DOI: 10.1021/ic200260r.

52 J. Zhang, N. Heinz and M. Dolg, Understanding Lanthanoid(III) Hydration Structure and Kinetics by Insights from Energies and Wave functions, *Inorg. Chem.*, 2014, **53**, 7700–7708, DOI: 10.1021/ic500991x.

53 A. S. Gugushe, A. Mpupa, T. S. Munonde, L. Nyaba and P. N. Nomngongo, Adsorptive Removal of Cd, Cu, Ni and Mn from Environmental Samples Using Fe_3O_4-ZrO_2@APS Nanocomposite: Kinetic and Equilibrium Isotherm

Studies, *Molecules*, 2021, **26**, 3209, DOI: 10.3390/molecules26113209.

54 A. Khamwichit, W. Dechapanya and W. Dechapanya, Adsorption kinetics and isotherms of binary metal ion aqueous solution using untreated venus shell, *Heliyon*, 2022, **8**, e09610, DOI: 10.1016/j.heliyon.2022.e09610.

55 C. Lei, B. Yan, T. Chen and X.-M. Xiao, Preparation and adsorption characteristics for heavy metals of active silicon adsorbent from leaching residue of lead-zinc tailings, *Environ. Sci. Pollut. Res.*, 2018, **25**, 21233–21242 https://link.springer.com/article/10.1007/s11356-018-2194-9.

56 A. A. Khedr, M. E. Fawzy, H. M. Ahmed, S. O. Alshammari and M. A. El-Khateeb, Treatment of heavy metal ions from simulated water using adsorption process via modified iron magnetic nanocomposite, *Desalin. Water Treat.*, 2024, **317**, 100071, DOI: 10.1016/j.dwt.2024.100071.